

1 **Effect of Oblique Electromagnetic Ion Cyclotron Waves on**  
2 **Relativistic Electron Scattering: CRRES Based Calculation**

3 G. V. Khazanov

4 NASA, Marshall Space Flight Center, Huntsville, Alabama, USA

5 K. V. Gamayunov

6 NASA, Marshall Space Flight Center, Huntsville, Alabama, USA

7 Short title: RB ELECTRON SCATTERING BY EMIC WAVES

8       **Abstract.** We consider the effect of oblique EMIC waves on relativistic electron  
9 scattering in the outer radiation belt using simultaneous observations of plasma and  
10 wave parameters from CRRES. The main findings can be summarized as follows: 1. In  
11 comparison with field-aligned waves, intermediate and highly oblique distributions  
12 decrease the range of pitch-angles subject to diffusion, and reduce the local scattering  
13 rate by an order of magnitude at pitch-angles where the principle  $|n| = 1$  resonances  
14 operate. Oblique waves allow the  $|n| > 1$  resonances to operate, extending the range  
15 of local pitch-angle diffusion down to the loss cone, and increasing the diffusion at  
16 lower pitch-angles by orders of magnitude; 2. The local diffusion coefficients derived  
17 from CRRES data are qualitatively similar to the local results obtained for prescribed  
18 plasma/wave parameters. Consequently, it is likely that the bounce-averaged diffusion  
19 coefficients, if estimated from concurrent data, will exhibit the dependencies similar  
20 to those we found for model calculations; 3. In comparison with field-aligned waves,  
21 intermediate and highly oblique waves decrease the bounce-averaged scattering rate  
22 near the edge of the equatorial loss cone by orders of magnitude if the electron energy  
23 does not exceed a threshold ( $\sim 2 - 5$  MeV) depending on specified plasma and/or  
24 wave parameters; 4. For greater electron energies, oblique waves operating the  $|n| > 1$   
25 resonances are more effective and provide the same bounce-averaged diffusion rate near  
26 the loss cone as field-aligned waves do.

## 27 1. Introduction

28 The flux of outer zone relativistic electrons (above 1 MeV) is extremely variable  
29 during geomagnetic storms. The competition between source and loss, both of which are  
30 enhanced during storm periods, determines the resulting relativistic electron flux level  
31 in the Earth's outer radiation belt (RB) [e. g., *Summers et al.*, 2004; *Reeves et al.*, 2003;  
32 *Green et al.*, 2004]. Usually, the flux falls by up to two or three orders of magnitude  
33 during main phase, and gradually increases over a period of a few days during storm  
34 recovery phase [e. g., *Meredith et al.*, 2002]. Analyzing 256 geomagnetic storms during  
35 the period 1989–2000, *Reeves et al.* [2003] found that 53 % of storms lead to higher flux  
36 during the storm recovery phase in comparison to pre-storm levels; 28 % produce no  
37 change; and 19 % lead to net decrease in flux. The large electron flux decrease during  
38 the main storm phase is usually associated with a decrease of  $Dst$  when the relativistic  
39 electrons adiabatically respond to the stretching of the magnetic field lines caused by  
40 the formation of a partial ring current (RC) [*Kim and Chan*, 1997], and/or a drift  
41 out the magnetopause boundary [*Li et al.*, 1997], and/or nonadiabatic scattering into  
42 the loss cone due to cyclotron interaction with electromagnetic ion cyclotron (EMIC)  
43 waves [*Thorne and Kennel*, 1971; *Lyons and Thorne*, 1972; *Summers and Thorne*,  
44 2003; *Albert*, 2003; *Thorne et al.*, 2005] and/or whistler-mode chorus/hiss waves [e. g.,  
45 *Summers et al.*, 2007].

46 Precipitation of outer RB electrons due to resonant pitch-angle scattering by  
47 EMIC waves is considered to be one of the most important loss mechanisms. Recently,

48 data from balloon-borne X-ray instruments provided indirect but strong evidence for  
49 the ability of EMIC waves to cause precipitation of outer zone relativistic electrons in  
50 the late afternoon-dusk MLT sector [Foat *et al.*, 1998; Lorentzen *et al.*, 2000; Millan  
51 *et al.*, 2002]. These observations stimulated theoretical and statistical studies which  
52 demonstrated that this mechanism of MeV electron pitch-angle diffusion can operate in  
53 the limit of strong diffusion, and can compete with adiabatic depletion caused by the  
54 *Dst* effect during the initial and main phases of storm [Summers and Thorne, 2003;  
55 Albert, 2003; Loto'aniu *et al.*, 2006; Meredith *et al.*, 2003].

56 Although the effectiveness of relativistic electron scattering depends strongly on  
57 EMIC wave spectral properties, unrealistic assumptions regarding the wave angular  
58 spread were made in previous theoretical studies. Namely, only strictly field-aligned or  
59 quasi field-aligned waves were considered as a driver for electron precipitation [e. g.,  
60 Summers and Thorne, 2003; Albert, 2003; Loto'aniu *et al.*, 2006]. The effect of oblique  
61 EMIC waves on relativistic electron scattering was recently discussed by Glauert and  
62 Horne [2005]. For prescribed plasma and wave parameters, considering the  $H^+$ -mode  
63 EMIC waves, they calculated the equatorial diffusion coefficients and demonstrated that  
64 when a realistic angular spread of propagating waves is taken into account, electron  
65 diffusion at  $\sim 0.5$  MeV is only slightly reduced compared with the assumption of  
66 field-aligned propagation, but at  $\sim 5$  MeV, electron diffusion at pitch-angles near  $90^\circ$   
67 is reduced by a factor of 5 and increased by several orders of magnitude at pitch-angles  
68  $30^\circ - 80^\circ$ . As a result, EMIC waves should flatten the pitch-angle distribution.

69 Thus, at energies of a few MeV, the assumption of field-aligned propagation

70 breaks down, significantly overestimating the pitch-angle diffusion coefficient at large  
71 pitch-angles, while underestimating the local diffusion rate at smaller pitch-angles by  
72 orders of magnitude. This is a very strong effect, so in contrast to [*Glauert and Horne,*  
73 2005], it is important to consider the impact of oblique EMIC waves on relativistic  
74 electron scattering using simultaneous observations for plasma/wave parameters, and  
75 to estimate the effect of bounce averaging. In the present study we calculate the  
76 pitch-angle diffusion coefficients using plasma and wave parameters observed by the  
77 Combined Release and Radiation Effects Satellite (CRRES) as reported by *Loto'aniu et*  
78 *al.* [2006].

79 This article is organized as follows: In section 2 we verify the pitch-angle diffusion  
80 coefficient calculations comparing our results with published results for both the  
81 equatorial and bounce-averaged scattering rates. Then, using model wave spectra for  
82  $He^+$ -mode EMIC waves with defined plasma parameters, we consider the effect of the  
83 wave normal angle distribution on relativistic electron scattering. In section 3, using  
84 plasma/wave parameters observed by CRRES [*Loto'aniu et al., 2006*], we present the  
85 results of our calculations and analysis of the local pitch-angle diffusion coefficients for  
86 two selected wave packets. Finally, in section 4 we summarize the main findings of our  
87 study.

## 88 2. Equatorial and Bounce–Averaged Pitch–Angle Diffusion

### 89 Coefficients: Model Calculations

An extensive statistical analysis of the EMIC events presented by *Meredith et al.* [2003], showed that most of the cases when the minimum resonant electron energy fell below 2 MeV were associated with wave frequencies just below the  $He^+$  gyrofrequency. So we take into account only the  $He^+$ -mode EMIC waves in the present study. The model wave frequency spectrum is assumed to be Gaussian,

$$B^2(\omega) \sim \exp\left\{-\frac{(\omega - \omega_m)^2}{\delta\omega^2}\right\}, \quad \omega_{LC} \leq \omega \leq \omega_{UC}, \quad (1)$$

where, following *Summers and Thorne* [2003] and/or *Albert* [2003],  $\omega_{LC} = \omega_m - \delta\omega$ ,  $\omega_{UC} = \omega_m + \delta\omega$ ,  $\omega_m = 3\Omega_{O^+}$ ,  $\delta\omega = 0.5\Omega_{O^+}$ , and  $\Omega_{O^+}$  is the gyrofrequency of  $O^+$ . In our calculations, the wave normal angle distribution,  $g(\theta)$ , is assumed to be a constant inside a specified region and zero otherwise. Below we consider the following three cases,

$$\begin{aligned} \text{Case A (field – aligned)} : \quad & 0^\circ \leq \theta < 30^\circ, \quad 150^\circ < \theta \leq 180^\circ, \\ \text{Case B (intermediate)} : \quad & 30^\circ \leq \theta < 60^\circ, \quad 120^\circ < \theta \leq 150^\circ, \\ \text{Case C (oblique)} : \quad & 60^\circ \leq \theta \leq 89^\circ, \quad 91^\circ \leq \theta \leq 120^\circ, \end{aligned} \quad (2)$$

where  $\theta$  is the wave normal angle. Note that the diffusion coefficient is a linear functional of the wave spectral density, and the sum of cases A, B, and C describe a situation when EMIC wave energy is evenly distributed over the entire wave normal angle region  $0^\circ \leq \theta \leq 180^\circ$  (we excluded the region near  $90^\circ$  because of Landau damping by thermal electrons [e. g., *Thorne and Horne*, 1992; *Khazanov et al.*, 2007]). For benchmark

purposes, we calculate also the diffusion coefficients for a Gaussian distribution over  $x = \tan \theta$  ( $0^\circ \leq \theta \leq 15^\circ$ ) which has been used by *Albert* [2003]. In each case, the wave amplitude is normalized to ensure

$$\int_{\omega_{LC}}^{\omega_{UC}} d\omega \int_0^\pi d\theta B^2(\omega) g(\theta) = 1 \text{ nT}^2. \quad (3)$$

90 Finally, to specify the ion content we follow *Summers and Thorne* [2003], *Albert* [2003],  
 91 *Meredith et al.* [2003], *Loto'aniu et al.* [2006], and prescribe the ion composition to be  
 92 70%  $H^+$ , 20%  $He^+$ , and 10%  $O^+$  (following [*Meredith et al.*, 2003] we call it a “storm  
 93 time” ion composition).

The results obtained using the relativistic version of the diffusion coefficient code of *Khazanov et al.* [2003] are shown in Figure 1. The first row shows the equatorial pitch-angle diffusion coefficients, the second row shows the corresponding resonance numbers averaged with the following weights:

$$\langle n(E, \alpha) \rangle = \frac{\sum_n n \left( \int_{\omega_{LC}}^{\omega_{UC}} d\omega \int_0^\pi d\theta D_{\alpha\alpha}^n(\omega, \theta, E, \alpha) \right)}{\sum_n \left( \int_{\omega_{LC}}^{\omega_{UC}} d\omega \int_0^\pi d\theta D_{\alpha\alpha}^n(\omega, \theta, E, \alpha) \right)}, \quad (4)$$

94 where  $E$  and  $\alpha$  are the electron kinetic energy and local pitch-angle, and  $D_{\alpha\alpha}^n(\omega, \theta, E, \alpha)$   
 95 is the partial equatorial pitch-angle diffusion coefficient, and the third row shows the  
 96 bounce-averaged diffusion coefficients. Note that resonances  $\pm n$  come together because  
 97 the  $\omega$ -term can be omitted in the quasilinear resonance condition,  $\omega - k_{\parallel} v_{\parallel} - n\Omega_e/\gamma = 0$ ,  
 98 [e. g., *Summers and Thorne*, 2003], and because the wave spectra are symmetric over  
 99  $\theta = 90^\circ$ . The “Gauss” lines in Figure 1 show the results for a Gaussian distribution  
 100 over  $x$ , and reproduce well the equatorial and bounce-averaged diffusion coefficients by  
 101 *Albert* [2003, Figure 6].

Figure 1

102 Let us first analyze the equatorial pitch-angle diffusion coefficients. For all energies,  
 103 Case A is only slightly less than “Gauss” if only  $|n| = 1$  resonances operate, but in the  
 104 region of  $|n| > 1$  it is about 5 times greater (Figure 1(c) and 1(d), the first row). These  
 105 dependencies are in good agreement with the previous results by *Albert* [2003, Figure 10,  
 106 the second row]. For both “Gauss” and Case A, as follows from the second row in the  
 107 Figure 1, the contributions from  $n < 0$  are negligible compared to  $n > 0$ , especially  
 108 for lower electron energies (see Figure 1(a) and 1(b), the second row). Cases B and C  
 109 further increase the EMIC wave normal angle, and as a result, suppress the  $|n| = 1$   
 110 resonances, and for low energies substantially shrink the region of pitch-angles subject  
 111 to diffusion (see Figure 1(a) and 1(b), the first row). At the same time, they increase by  
 112 orders of magnitude the contribution from  $|n| > 1$ , which operate for greater electron  
 113 energies, and cover a greater pitch-angle region (see Figure 1(c) and 1(d), the first row).  
 114 The growing contribution of the  $n < 0$  resonances is more pronounced in Cases B and  
 115 C (in comparison to Case A) because EMIC waves become more elliptically polarized  
 116 with increasing wave normal angle (see Figure 1, the second row).

117 Overall, in comparison with the field-aligned waves, the intermediate and highly  
 118 oblique wave distributions decrease the pitch-angle range subjected to diffusion, and  
 119 reduce the equatorial scattering rate by orders of magnitude for low energy electrons  
 120 ( $E < 2$  MeV) when only principle  $|n| = 1$  resonances operate. For greater electron  
 121 energies, the  $|n| = 1$  resonances operate only in a narrow region at large pitch-angles,  
 122 and despite their greater contribution from field-aligned waves, cannot support the local  
 123 electron diffusion into the loss cone. In this case, oblique waves operate on the  $|n| > 1$



124 resonances more effectively, and extend the range of pitch-angle diffusion down to the  
 125 loss cone. Note that despite our inclusion of the  $He^+$ -mode, the above results are in  
 126 qualitative agreement with the results of *Glauert and Horne* [2005, Figures 6 and 7]  
 127 obtained for the equatorial pitch-angle scattering by the  $H^+$ -mode EMIC waves.

128 Now we consider the effect of bounce averaging on pitch-angle diffusion coefficients.  
 129 To calculate the bounce-averaged diffusion coefficients, we utilize all the plasma/wave  
 130 parameters used in the above calculation of the equatorial coefficients, and in addition,  
 131 a dipole magnetic field model, and the meridional density distribution from [*Khazanov*  
 132 *et al.*, 2006]. We further assume that the EMIC waves are confined to mirror points,  
 133 and the wave spectra are equatorial.

134 In all considered cases (2), the bounce averaging does not change the shape of the  
 135 diffusion coefficients for energies below 2 MeV (compare the first and third rows in  
 136 Figure 1) but simply reduces the pitch-angle diffusion rates by an order of magnitude.  
 137 For energies 5 and 10 MeV, the peak values of the bounce-averaged diffusion coefficients  
 138 are lower by about a factor of 3 than in the first row of Figure 1. However, the  
 139 bounce-averaged results for  $E > 2$  MeV differ qualitatively from the local coefficients  
 140 for all wave normal distributions. Due to significant scattering at higher latitudes, the  
 141 bounce-averaged diffusion coefficients extend further into the loss cone compared to  
 142 equatorial results. The bounce-averaged results in Figure 1 demonstrate clearly the  
 143 effect of EMIC wave normal angle distribution on relativistic electron scattering.

144 Recently, *Shprits et al.* [2006] showed that the electron lifetime is most sensitive to  
 145 the value of the bounce-averaged scattering rate near the edge of the equatorial loss

146 cone, whose value is used to estimate the electron loss timescale [e. g., *Summers et al.*,  
147 2007]. Considering the third row in Figures 1(a), 1(b), we can see that the intermediate  
148 and highly oblique wave distributions reduce the scattering rate near the loss cone by  
149 orders of magnitude because only principal  $|n| = 1$  resonances operate. For higher  
150 electron energies (Figures 1(c), 1(d)) when  $|n| > 1$  resonances start to operate, the  
151 pitch-angle scattering near the edge of the equatorial loss cone depends only slightly  
152 on the wave normal angle distribution, resulting in nearly the same bounce-averaged  
153 diffusion rate for all cases. In other words, there is an electron energy, depending on  
154 specified plasma and/or wave parameters, which separates lower and higher energy  
155 regions with different EMIC wave scattering properties. In the lower energy region,  
156 using a field-aligned wave normal angle distribution leads to a significant overestimate of  
157 the diffusion rate compared to oblique waves. In the higher energy region, the scattering  
158 rate near the edge of the loss cone almost does not depend on the wave normal angle  
159 distribution.

### 160 **3. Local Pitch-Angle Diffusion Coefficient: CRRES Based** 161 **Calculations**

#### 162 **3.1. Minimum Resonant Energy**

163 Recently, *Meredith et al.* [2003] presented an extensive statistical analysis of over  
164 800 EMIC events observed on CRRES to establish whether electron scattering can occur  
165 at geophysically interesting energies ( $\leq 2$  MeV). In the absence of specific information

166 on the wave normal angle, the dispersion relation for strictly field-aligned propagating  
 167 EMIC waves was used to obtain the electron resonant energy. For consistency, *Meredith*  
 168 *et al.* [2003] included only waves with a high ellipticity ( $|\epsilon| \geq 0.3$ ) in the survey.  
 169 This yielded a subset of 416 events, the majority of which were identified as L-mode.  
 170 Considering only the central wave frequency,  $\omega_m$ , in each wave packet, *Meredith et al.*  
 171 [2003] found that in about 11 % of the observations, the electron minimum resonant  
 172 energy fell below 2 MeV. These cases were restricted to regions where  $\omega_{pe}/\Omega_e > 10$ , and  
 173 were associated with wave frequencies just below the helium or proton gyrofrequencies.  
 174 More recently, trying to increase the above percentage, *Loto'aniu et al.* [2006] considered  
 175 the entire frequency range for each of 25 EMIC wave packets observed on CRRES during  
 176 the initial phase of a geomagnetic storm on 11 August, 1991. These authors also used  
 177 the dispersion relation for strictly parallel propagating EMIC waves, and found that in  
 178 comparison with results utilizing  $\omega_m$  only, there are 3 to 4 times more wave packets that  
 179 are able to interact with electrons below 2 MeV.

The minimum resonant energy depends on the wave normal angle, and the  
 dependency is stronger in vicinity of the resonant frequencies where the wave number  
 grows especially fast. Omitting the  $\omega$ -term in a quasilinear resonance condition  
 ( $\omega - k_{\parallel}v_{\parallel} - n\Omega_e/\gamma = 0$ ) and taking  $n = 1$ , we can obtain the minimum kinetic energy  
 required by electrons for cyclotron resonance interaction with EMIC waves,

$$\frac{E_{min}}{m_e c^2} = \frac{1}{\sqrt{1 - \left(\frac{v}{c}\right)^2}} - 1, \quad \left(\frac{v}{c}\right)^2 = \frac{1}{1 + \cos^2 \theta \left(\frac{kc}{\Omega_e}\right)^2}, \quad (5)$$

180 where  $E_{min}$  is the minimum kinetic energy,  $m_e$  is the electron rest mass,  $c$  is the speed

181 of light, and  $k$  and  $v$  are the wave number and electron velocity. Note that equation  
 182 (5) can be obtained from equation (7) of *Summers and Thorne* [2003] by omitting the  
 183 two smallest terms in their equation. To calculate the electron minimum energy, we  
 184 select the plasma parameters reported by *Loto'aniu et al.* [2006, Wave packet # 16],  
 185 and the results of our calculation are presented in Figure 2. For  $\theta = 0^\circ$ , as reported  
 186 in many previous studies [e. g., *Summers and Thorne*, 2003], in order to get lower  
 187  $E_{min}$ , the required wave frequency has to be closer to the  $He^+$  gyrofrequency (in other  
 188 words, the wave number should be greater). For most wave normal angles, increasing  
 189 the angle slightly also increases the minimum energy but there is a dramatic decrease  
 190 of  $E_{min}$  in the region near  $\theta = 90^\circ$ . This transition boundary depends on the wave  
 191 frequency. Indeed, there is a resonant wave normal angle (the angle at which the wave  
 192 number becomes infinite in the “cold plasma” approximation) for any frequency in  
 193 the range between  $\Omega_{He^+}$  and the corresponding bi-ion frequency, and this angle is  
 194 closer to  $\theta = 0^\circ$  if the wave frequency is closer to  $\Omega_{He^+}$ . Because of the wave number  
 195 increase, the resonant energy decreases dramatically in the vicinity of the resonant  
 196 wave normal angle, an effect clearly observed in Figure 2. So in cold plasma,  $E_{min}$  is  
 197 lower for oblique or highly oblique wave propagation, depending on wave frequency,  
 198 than for strictly field-aligned propagating EMIC waves. But, of course, the diffusion  
 199 coefficient for those wave normal angles should be significant in order to determine the  
 200 “physically meaningful”  $E_{min}$ , and moreover the cyclotron damping in vicinity of the  
 201  $He^+$  gyrofrequency can be very strong (see below).

Figure 2

### 202 3.2. Pitch–Angle Diffusion Coefficient

203 It was demonstrated in section 2 that oblique wave propagation can strongly  
 204 change the effectiveness of both the local and bounce–averaged relativistic electron  
 205 scatterings. At the same time, those results were obtained for plasma parameters  
 206 and wave spectra which were specified independently. So it is important to consider  
 207 the effect of using concurrent observational data. In contrast to section 2, we now  
 208 calculate the local pitch–angle diffusion coefficients using the data for plasma and wave  
 209 parameters reported by *Loto’aniu et al.* [2006].

210 A long duration wave event was observed by CRRES on 11 August, 1991 in the  
 211 interval  $\sim 0500 - 0700$  UT (14.4 – 15.8 MLT) over a magnetic latitude range of  $-26^\circ$  to  
 212  $-24^\circ$  and  $L=6.3-7.6$ . CRRES was close to apogee in the plasmatrough, and the electron  
 213 density varied slowly from 12 to 17  $\text{cm}^{-3}$ . A total of 25 EMIC wave packets were  
 214 identified both below and above the local  $He^+$  gyrofrequency [*Loto’aniu et al.*, 2006].  
 215 In order to estimate the spectral properties of the wave packets, these authors fitted  
 216 a Gaussian distribution to the static wave packet transverse power spectral density.  
 217 Typical FFT data windows and frequency resolutions for the static spectrograms  
 218 were 100 s and 0.02 Hz, respectively. The Gaussian function fit provided the central  
 219 frequencies,  $\omega_m$ , and the spectral semibandwidths,  $\delta\omega$ . The total wave magnetic power,  
 220  $\delta B^2$ , was estimated for each wave packet by summing the power spectral density bins in  
 221 the range  $\omega_m \pm \delta\omega$  and then multiplying the result by  $\delta\omega$ . Using the full wave spectral  
 222 range, *Loto’aniu et al.* [2006] found that electrons with  $E \leq 2$  MeV could interact with

223 only three wave packets (16, 17, and 19) if stormtime ion concentration was assumed  
 224 (70%  $H^+$ , 20%  $He^+$ , and 10%  $O^+$ ). Those packets were the  $He^+$ -mode EMIC waves,  
 225 and for the calculation below we selected two of them. The associated plasma and wave  
 226 characteristics are summarized in Table 1. Note that to generate this Table we used the Table 1  
 227 definition of full-width at half maximum (FWHM) as it was given by *Loto'aniu et al.*  
 228 [2006], i. e.,  $FWHM = 2\sqrt{2\ln 2}\delta\omega$ , despite the Gaussian fit  $\sim \exp\{-(\omega - \omega_m)^2 / \delta\omega^2\}$ .  
 229 Of the packets 16, 17, and 19, wave packet 16 has the most narrow and 19 the widest  
 230 distributions, with corresponding power spectral densities presented in Figure 3. Figure 3

231 To show the effect of the wave normal angle distribution on relativistic electron  
 232 scattering, we use the wave normal angle distributions (2), and in addition, a stormtime  
 233 ion concentration is assumed. For reference purposes, we also calculate the diffusion  
 234 coefficients for strictly parallel/antiparallel propagating EMIC waves. For each wave  
 235 packet, the power spectral density is normalized to the corresponding wave magnetic  
 236 power  $\delta B^2$  shown in Table 1, and this normalization is kept the same for any particular  
 237 wave normal angle distribution (2). In order to estimate the minimum resonant energy  
 238 we use  $y_{UC}$  from Table 1. For strictly field-aligned wave propagation, as follows from  
 239 Figure 2, the energy is about 2 MeV for both wave packets (we can use Figure 2 for  
 240 wave packet 19 because  $\omega_{pe}/\Omega_e$  was nearly the same during both). This minimum  
 241 resonant energy exceeds the values presented by *Loto'aniu et al.* [2006], especially  
 242 for wave packet 16; for this packet and a stormtime ion concentration, they obtained  
 243  $E_{min} = 0.2$  MeV that, as follows from Figure 2, corresponds to a  $y_{UC}$  about 0.2496.

244 Figure 4 shows the results of our calculation for wave packet 16. For strictly Figure 4

245 parallel wave propagation the minimum resonant energy is only slightly below 2 MeV,  
 246 and the diffusion coefficients for field-aligned and intermediate wave propagation are  
 247 only nonzero in Figures 4(c) and 4(d). Cases A and B demonstrate results similar to  
 248 Figures 1(b) and 1(c). Because  $y_{UC}$  is very close to the  $He^+$  gyrofrequency, the minimum  
 249 resonant energy falls below 1 MeV if the wave normal angle exceeds  $88^\circ$ , so that Case C  
 250 may potentially scatter such low energy electrons with an appreciable rate as shown in  
 251 Figures 4(a) and 4(b). Another feature of highly oblique waves is clearly observed in  
 252 Figures 4(d) where the range of pitch-angle diffusion is substantially extended down to  
 253 the loss cone. While Case C exhibits a quite different behavior compared to Figure 1,  
 254 there is a similarity between the diffusion coefficients in Figures 4(d) and 1(c).

255 The diffusion coefficients for wave packet 19 are shown in Figure 5. Both Figure 5(c) Figure 5  
 256 and 5(d) are quite similar, and demonstrate qualitatively the same behavior as in  
 257 Figures 1(a) and 1(b). As follows from Figures 5(a) and 5(b), Case C practically does  
 258 not scatter low energy electrons, mainly because of a lower  $y_{UC}$  for wave packet 19 than  
 259 in Figure 4.

### 260 3.3. Cyclotron Damping Near $He^+$ Gyrofrequency and Its Consequence for 261 Electron Scattering

As follows from Table 1,  $y_{UC}$  is very close to the local  $He^+$  gyrofrequency  
 ( $y_{He^+} = 0.25$ ) for both wave packets. In this frequency region, the  $He^+$ -mode  
 experiences strong cyclotron damping due to interaction with thermal  $He^+$  [e. g.,  
*Akhiezer et al.*, 1975]. To demonstrate this, we assume the  $He^+$  temperature to be

$T_{He^+} = 1$  eV, and present in Figure 6 the wave damping rate for the stormtime ion composition and plasma parameters observed during wave packet 16. The frequency range shown covers approximately the entire wave packet 16. The damping rate for  $y_{LC}$  has only narrow peak for  $\theta > 89^\circ$ , and this region is excluded from the calculation of the diffusion coefficients (see equation (2)). For  $y_m$ , the region of damping near ninety degrees extends slightly below  $89^\circ$ , and in addition, small damping appears for a field-aligned wave propagation. The situation becomes dramatically different for  $y_{UC}$  when the  $He^+$ -mode experiences strong damping in the entire wave normal angle region; the energy damping rate is  $0.5/\gamma_{He^+} \approx 7$  sec, which is only four times greater than the wave period. In all cases, substantial damping takes place only if  $|y - 0.25| \lesssim k_{\parallel} v_{\parallel, He^+} / \Omega_{H^+}$ , where  $v_{\parallel, He^+}$  is the field-aligned temperature of  $He^+$ . Moreover, we employ a “cold plasma” approximation in our diffusion coefficient software (as was done by *Loto'aniu et al.* [2006]), some must check the validity of this approximation. Particularly, the inequality

$$|y - 0.25| \gg \frac{k_{\parallel} v_{\parallel, He^+}}{\Omega_{H^+}} = \varepsilon_{th} \quad (6)$$

262 should hold.

263 Inequality (6) is extremely crucial for the diffusion coefficient calculation because  
 264 thermal effects should be considered if inequality (6) is violated, but more importantly,  
 265 the  $He^+$ -mode damps strongly in the region  $|y - 0.25| \lesssim \varepsilon_{th}$ . For wave packets 16 and  
 266 19, inequality (6) is strongly violated in the vicinity of  $y_{UC}$ , and waves cannot exist in  
 267 these frequency regions, which for  $T_{He^+} = 1$  eV, are the ranges  $\varepsilon_{th} = 5 \times 10^{-3} - 9 \times 10^{-2}$



268 and  $\varepsilon_{th} = 3 \times 10^{-3} - 6 \times 10^{-2}$ , respectively. Using these numbers and Table 1, we  
 269 conclude that in order to suppress cyclotron damping completely, the  $He^+$  temperature  
 270 should be decreased at least by  $1/80$  for wave packet 16, and at least by  $1/40$  for wave  
 271 packet 19. Any reasonable change to the temperature assumed in our calculation cannot  
 272 eliminate the effect, and can only influence the frequency range subject to cyclotron  
 273 damping.

274 Our conclusion that EMIC waves experience strong cyclotron damping near  
 275 the  $He^+$  gyrofrequency contradicts the results of *Loto'aniu et al.* [2006] because  
 276 these authors estimated all their  $y_{UC}$  values from CRRES data (after filtering,  
 277 FFT, and Gaussian approximations). Unfortunately we do not know all the details  
 278 regarding data processing used by *Loto'aniu et al.* [2006], but we know that the wave  
 279 frequency resolution in their data was 0.02 Hz. This uncertainty provides the ranges  
 280  $(y_{LC}, y_{UC}) = (0.20 - 0.25, 0.22 - 0.27)$  and  $(y_{LC}, y_{UC}) = (0.17 - 0.22, 0.22 - 0.27)$  for  
 281 wave packets 16 and 19, respectively, that can reconcile our theoretical result with  
 282 data reported by *Loto'aniu et al.* [2006]. So we do not see any reason inequality (6) is  
 283 violated, and it must be taken into account.

284 Let us now recalculate the diffusion coefficients presented in Figure 4, neglecting  
 285 contributions from all the partial diffusion coefficients if  $|y - 0.25| \leq \varepsilon_{th}$  (keeping all  
 286 parameters the same). Note that all the results presented in Figure 1 are still valid  
 287 because inequality (6) holds for all those parameters. The results of the recalculation  
 288 are presented in Figure 7, and there is a qualitative difference in comparison to Figure 4.  
 289 Now, for all wave normal angle distributions, low energy electron pitch-angle diffusion

Figure 7

290 is not possible, and while the 2 MeV diffusion coefficients are nonzero in Figure 7(c),  
 291 they are at least partly inside the equatorial loss cone for  $L \approx 7.3$ . For greater electron  
 292 energies, the contribution from the high frequency part of the wave power spectral  
 293 density decreases. As a result, Figures 7(d) and 4(d) look similar except that diffusion  
 294 vanishes at slightly lower pitch-angles in Figure 7(d) than in Figure 4(d), and the  
 295 transition between  $|n| = 1$  and  $|n| = 2$  resonances is not continued in Figure 7(d) for  
 296 Case A.

297 The results of our recalculation for wave packet 19 are shown in Figure 8. Similar  
 298 to wave packet 16, diffusion is not possible for low energies, and Figures 8(d) and 5(d)  
 299 are very similar.

Figure 8

300 In conclusion, we emphasize that as we demonstrated above, the  $He^+$ -mode  
 301 does not experience significant cyclotron damping by thermal  $He^+$  if  $y \lesssim y_m$  (see  
 302 Figure 6). So the observed changes in the diffusion coefficients are due to the frequency  
 303 region near  $y_{UC}$ , and qualitatively correct diffusion coefficients may be obtained by  
 304 only considering the region  $y \lesssim y_m$ . This result is consistent with the conclusions of  
 305 *Meredith et al.* [2003] regarding the electron minimum resonant energy which were  
 306 obtained by considering only the central wave packet frequencies, and suggests that the  
 307 number of EMIC wave packets that are able to interact with electrons below 2 MeV  
 308 may significantly decrease compared with the estimate of *Loto'aniu et al.* [2006].

## 309 4. Summary and Conclusions

310 Precipitation of outer RB electrons due to resonant pitch-angle scattering by  
 311 EMIC waves is considered to be one of the most important loss mechanisms. The  
 312 effectiveness of relativistic electron scattering depends strongly on the EMIC wave  
 313 spectral properties, but unrealistic assumptions regarding the wave angular spread  
 314 were made in previous theoretical studies. Namely, only strictly field-aligned or quasi  
 315 field-aligned waves were considered [*Summers and Thorne, 2003; Albert, 2003; Loto'aniu*  
 316 *et al., 2006*]. The effect of oblique EMIC waves on relativistic electron scattering  
 317 was recently discussed by *Glauert and Horne [2005]*. For prescribed plasma and wave  
 318 parameters, considering the  $H^+$ -mode EMIC waves, they calculated the local diffusion  
 319 coefficients and demonstrated that when a realistic angular spread of propagating waves  
 320 is taken into account, electron diffusion at  $\sim 0.5$  MeV is only slightly reduced compared  
 321 with the assumption of field-aligned propagation, but at  $\sim 5$  MeV, electron diffusion  
 322 at pitch-angles near  $90^\circ$  is reduced by a factor of 5 and increased by several orders of  
 323 magnitude at pitch-angles  $30^\circ - 80^\circ$ . Thus at energies of a few MeV the assumption of  
 324 field-aligned wave propagation breaks down, significantly overestimates the pitch-angle  
 325 diffusion coefficient at large pitch-angles, and underestimates the local diffusion rate at  
 326 smaller pitch-angles by orders of magnitude.

327 The purpose of the present study was to consider the impact of oblique EMIC  
 328 waves on local relativistic electron scattering using simultaneous observations of plasma  
 329 and wave parameters from CRRES, and to estimate the effect of bounce averaging.

330 Analyzing 25 EMIC wave packets, and considering the full wave spectral range,  
 331 *Loto'aniu et al.* [2006] found that electrons with  $E \leq 2$  MeV could interact with  
 332 wave packets 16, 17, and 19 only if a stormtime ion concentration is assumed (70%  
 333  $H^+$ , 20%  $He^+$ , and 10%  $O^+$ ). Those packets were  $He^+$ -mode EMIC waves, where we  
 334 have selected wave packets 16 and 19 for our analyzes. Results of our study can be  
 335 summarized as follows:

336 1. In comparison with the field-aligned waves, the intermediate and highly oblique  
 337 distributions slightly decrease the pitch-angle range subject to diffusion, and reduce the  
 338 local scattering rate by about an order of magnitude at pitch-angles where the principle  
 339  $|n| = 1$  resonances operate (see Figures 7 and 8). Oblique waves allow the  $|n| > 1$   
 340 resonances to operate, extending the range of local pitch-angle diffusion down to the  
 341 loss cone, and increasing the diffusion at lower pitch-angles by orders of magnitude (see  
 342 Figures 7(d)).

343 2. The local diffusion coefficients based on concurrent plasma/wave parameters from  
 344 CRRES are qualitatively similar to the results obtained for defined plasma parameters  
 345 with model wave spectra (compare Figures 7 and 8 with the first row in Figure 1). So we  
 346 anticipate that the bounce-averaged diffusion coefficients, if estimated from concurrent  
 347 wave/particle data, will exhibit dependencies similar to those we found for the model  
 348 bounce-averaged calculations (see Figure 1, the third row). Those dependencies are:

349 3. For low energy electrons, if only principal  $|n| = 1$  resonances operate, intermediate  
 350 and highly oblique wave distributions (in contrast to field-aligned waves) reduce the  
 351 equatorial pitch-angle range subject to diffusion, and decrease the bounce-averaged

352 scattering rate near the edge of the equatorial loss cone by orders of magnitude. This  
353 low energy threshold depends on specified plasma and/or wave parameters, which is  
354  $E \approx 2$  MeV for parameters used in Figure 1.

355 4. For greater electron energies, the  $|n| = 1$  resonances operate only in a narrow  
356 region at large pitch-angles (see Figures 1(c) and 1(d)), but due to significant scattering  
357 at higher latitudes, the bounce-averaged diffusion coefficients for field-aligned waves  
358 extend down to the equatorial loss cone. For these energies, oblique waves operating  
359 at  $|n| > 1$  resonances are more effective and provide nearly the same bounce-averaged  
360 scattering rate in the vicinity of the loss cone as field-aligned waves do (see Figures 1(c)  
361 and 1(d), the third row).

362 **Acknowledgments.** This research was performed while K. Gamayunov held a NASA  
363 Postdoctoral Program appointment at NASA/MSFC. Funding in support of this study was  
364 provided by NASA grant UPN 370-16-10, NASA HQ POLAR Project, and NASA LWS  
365 Program.

365 **References**

- 367 Akhiezer, A. I., I. A. Akhiezer, R. V. Polovin, A. G. Sitenko, and K. N. Stepanov (1975),  
368 *Plasma Electrodynamics*, vol. 1, Pergamon, Tarrytown, N. Y.
- 369 Albert, J. M. (2003), Evaluation of quasi-linear diffusion coefficients for EMIC waves in a  
370 multispecies plasma, *J. Geophys. Res.*, *108*, A6, 1249, doi:10.1029/2002JA009792.
- 371 Foat, J. E., R. P. Lin, D. M. Smith, F. Fenrich, R. Millan, I. Roth, K. R. Lorentzen,  
372 M. P. McCarthy, G. K. Parks, and J. P. Treilhou (1998), First detection of a  
373 terrestrial MeV X-ray burst, *Geophys. Res. Lett.*, *25*, 4109.
- 374 Glauert, S. A., and R. B. Horne (2005), Calculation of pitch angle and energy  
375 diffusion coefficients with the PADIE code, *J. Geophys. Res.*, *110*, A04206,  
376 doi:10.1029/2004JA010851.
- 377 Green, J. C., T. G. Onsager, T. P. O'Brien, and D. N. Baker (2004), Testing loss  
378 mechanisms capable of rapidly depleting relativistic electron flux in the Earth's  
379 outer radiation belt, *J. Geophys. Res.*, *109*, A12211, doi:10.1029/2004JA010579.
- 380 Khazanov, G. V., K. V. Gamayunov, D. L. Gallagher, and J. U. Kozyra (2006), Self-  
381 consistent model of magnetospheric ring current and propagating electromagnetic  
382 ion cyclotron waves: Waves in multi ion magnetosphere, *J. Geophys. Res.*, *111*,  
383 A10202, doi:10.1029/2006JA011833.
- 384 Khazanov, G. V., K. V. Gamayunov, D. L. Gallagher, J. U. Kozyra, and M. W.  
385 Liemohn (2007), Self-consistent model of magnetospheric ring current and  
386 propagating electromagnetic ion cyclotron waves. 2. Wave induced ring current

- 387 precipitation and thermal electron heating, *J. Geophys. Res.*, *112*, A04209,  
388 doi:10.1029/2006JA012033.
- 389 Khazanov, G. V., K. V. Gamayunov, and V. K. Jordanova, Self-consistent model  
390 of magnetospheric ring current ions and electromagnetic ion cyclotron  
391 waves: The 2–7 May 1998 storm (2003), *J. Geophys. Res.*, *108*, A12, 1419,  
392 doi:10.1029/2003JA009856.
- 393 Kim, H.-J., and A. A. Chan, Fully adiabatic changes in storm time relativistic electron  
394 fluxes (1997), *J. Geophys. Res.*, *102*, 22107.
- 395 Li, X., D. N. Baker, M. Temerin, T. E. Cayton, G. D. Reeves, R. A. Christiansen, J. B.  
396 Blake, M. D. Looper, R. Nakamura, and S. G. Kanekal (1997), Multi-satellite  
397 observations of the outer zone electron variation during the November 3–4, 1993,  
398 magnetic storm, *J. Geophys. Res.*, *102*, 14123.
- 399 Lorentzen, K. R., M. P. McCarthy, G. K. Parks, J. E. Foat, R. M. Millan, D. M. Smith,  
400 R. P. Lin, and J. P. Treilhou (2000), Precipitation of relativistic electrons by  
401 interaction with electromagnetic ion cyclotron waves, *J. Geophys. Res.*, *105*,  
402 5381.
- 403 Loto'aniu, T. M., R. M. Thorne, B. J. Fraser, and D. Summers (2006), Estimating  
404 relativistic electron pitch angle scattering rate using properties of the  
405 electromagnetic ion cyclotron wave spectrum, *J. Geophys. Res.*, *111*, A04220,  
406 doi:10.1029/2005JA011452.
- 407 Lyons, L. R., and R. M. Thorne (1972), Parasitic pitch angle diffusion of radiation belt  
408 particles by ion cyclotron waves *J. Geophys. Res.*, *77*, 5608.

- 409 Meredith, N. P., R. B. Horne, D. Summers, R. M. Thorne, R. H. A. Iles, D. Heynderickx,  
410 and R. R. Anderson (2002), Evidence for acceleration of outer zone electrons to  
411 relativistic energies by whistler mode chorus, *Ann. Geophys.*, *20*, 967.
- 412 Meredith, N. P., R. M. Thorne, R. B. Horne, D. Summers, B. J. Fraser, and R. R.  
413 Anderson (2003), Statistical analysis of relativistic electron energies for cyclotron  
414 resonance with EMIC waves observed on CRRES, *J. Geophys. Res.*, *108*, A6,  
415 1250, doi:10.1029/2002JA009700.
- 416 Millan, R. M., R. P. Lin, D. M. Smith, K. R. Lorentzen, and M. P. McCarthy (2002), X-  
417 ray observations of MeV electron precipitation with a balloon-borne germanium  
418 spectrometer, *Geophys. Res. Lett.*, *29*(24), 2194, doi:10.1029/2002GL015922.
- 419 Reeves, G. D., K. L. McAdams, R. H. W. Friedel, and T. P. O'Brien (2003), Acceleration  
420 and loss of relativistic electrons during geomagnetic storms, *Geophys. Res. Lett.*,  
421 *30*(10), 1529, doi:10.1029/2002GL016513.
- 422 Shprits, Y. Y., W. Li, and R. M. Thorne (2006), Controlling effect of the pitch angle  
423 scattering rates near edge of the loss cone on electron lifetimes, *J. Geophys. Res.*,  
424 *111*, A12206, doi:10.1029/2006JA011758.
- 425 Summers, D., C. Ma, and T. Mukai (2004), Competition between acceleration and loss  
426 mechanisms of relativistic electrons during geomagnetic storms, *J. Geophys. Res.*,  
427 *109*, A04221, doi:10.1029/2004JA010437.
- 428 Summers, D., B. Ni, and N. P. Meredith (2007), Timescales for radiation belt electron  
429 acceleration and loss due to resonant wave-particle interactions: 2. Evaluation  
430 for VLF chorus, ELF hiss, and electromagnetic ion cyclotron waves, *J. Geophys.*



- 431 *Res.*, 112, A04207, doi:10.1029/2006JA011993.
- 432 Summers, D., and R. M. Thorne (2003), Relativistic electron pitch-angle scattering  
433 by electromagnetic ion cyclotron waves during geomagnetic storms, *J. Geophys.*  
434 *Res.*, 108, A4, doi:10.1029/2002JA009489.
- 435 Thorne, R. M., and R. B. Horne (1992), The contribution of ion-cyclotron waves to  
436 electron heating and SAR-arcs excitation near the storm-time plasmapause,  
437 *Geophys. Res. Lett.*, 19, 417.
- 438 Thorne, R. M., R. B. Horne, S. A. Glauert, N. P. Meredith, Y. Y. Shprits, D.  
439 Summers, and R. R. Anderson (2005), The influence of wave-particle interactions  
440 on relativistic electron dynamics during storms, in *Inner Magnetosphere*  
441 *Interactions: New Perspectives From Imaging*, *Geophys. Monogr. Ser.*, vol. 159,  
442 edited by J. Burch, M. Schulz, and M. Spence, pp. 101–112, AGU, Washington,  
443 D. C.
- 444 Thorne, R. M., and C. F. Kennel (1971), Relativistic electron precipitation during  
445 magnetic storm main phase, *J. Geophys. Res.*, 76, 4446.
- 
- 446 K. V. Gamayunov, National Space Science and Technology Center, NASA Marshall  
447 Space Flight Center, Space Science Department, 320 Sparkman Drive, Huntsville, AL  
448 35805, USA. (e-mail: konstantin.gamayunov@msfc.nasa.gov)
- 449 G. V. Khazanov, National Space Science and Technology Center, NASA Marshall  
450 Space Flight Center, Space Science Department, 320 Sparkman Drive, Huntsville, AL  
451 35805, USA. (e-mail: george.khazanov@msfc.nasa.gov)

452 Received \_\_\_\_\_

**Figure 1.** Equatorial and bounce-averaged diffusion coefficients versus equatorial pitch-angle for scattering relativistic electrons by the  $He^+$ -mode of EMIC waves. Spectral parameters and ion content are given in the text.  $L=4$ , and  $(\omega_{pe}/\Omega_e)^2 = 10^3$ , where  $\omega_{pe}$  and  $\Omega_e$  are the equatorial electron plasma frequency and gyrofrequency (without Lorentz factor), respectively. The curve “Gauss” is for a wave normal angle distribution adopted by *Albert [2003]*. The second row shows the average resonant number weighted by the partial equatorial diffusion coefficient (see the text for definition).

**Figure 2.** Minimum resonant energy versus normal angle of the  $He^+$ -mode EMIC waves. The plasma density and magnetic field are  $17 \text{ cm}^{-3}$  and  $171 \text{ nT}$ , taken from [*Loto’aniu et al., 2006, Wave packet # 16*]. The ion composition is 70%  $H^+$ , 20%  $He^+$ , and 10%  $O^+$ , and the normalized wave frequency is defined as  $y = \omega/\Omega_{H^+}$ .

**Figure 3.** Transverse power spectral densities for wave packets 16 and 19 obtained by *Loto’aniu et al. [2006]*. The solid and dashed vertical lines restrict the frequency range  $\omega_m \pm \delta\omega$  for packets 16 and 19, respectively.

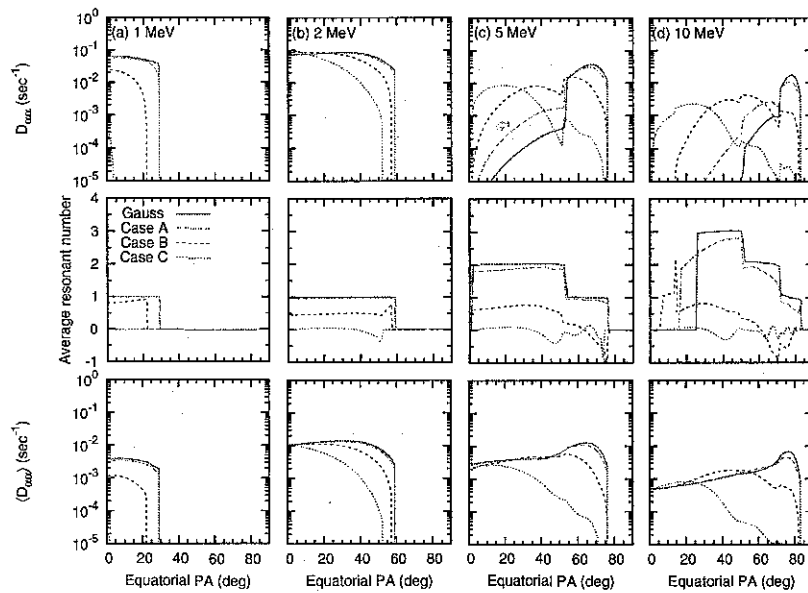
**Figure 4.** Local pitch-angle diffusion coefficients for wave packet 16. Calculations are based on a stormtime ion composition,  $\eta_{H^+} = 0.7$ ,  $\eta_{He^+} = 0.2$ , and  $\eta_{O^+} = 0.1$ . “W/P 16” shows the results for strictly parallel-antiparallel propagating  $He^+$ -modes, and Cases A, B, and C are obtained for the corresponding wave normal angle distribution given by (2).

**Figure 5.** Same as Figure 4, except for wave packet 19.

**Figure 6.** The  $He^+$ -mode damping rate due to interaction with thermal  $He^+$ . The phase space distribution function for  $He^+$  is Maxwellian with  $T_{He^+} = 1$  eV, but thermal effects are neglected in the real part of the dispersion relation. All other plasma species are described in a “cold plasma” approximation. A stormtime ion composition is assumed, and the plasma density and magnetic field are taken from [Loto'aniu et al., 2006, Wave packet # 16].

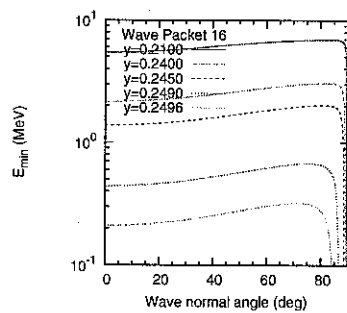
**Figure 7.** Same as Figure 4, except inequality  $|y - 0.25| > k_{\parallel} v_{\parallel, He^+} / \Omega_{H^+}$  is held during the diffusion coefficient calculations.

**Figure 8.** Same as Figure 5, except inequality  $|y - 0.25| > k_{\parallel} v_{\parallel, He^+} / \Omega_{H^+}$  is held during the diffusion coefficient calculations.



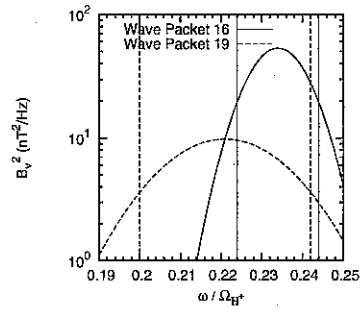
461

462 **Figure 1.**



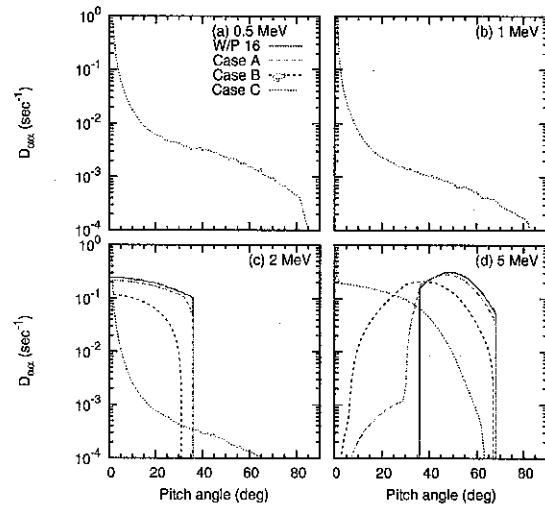
463

464 **Figure 2.**



465

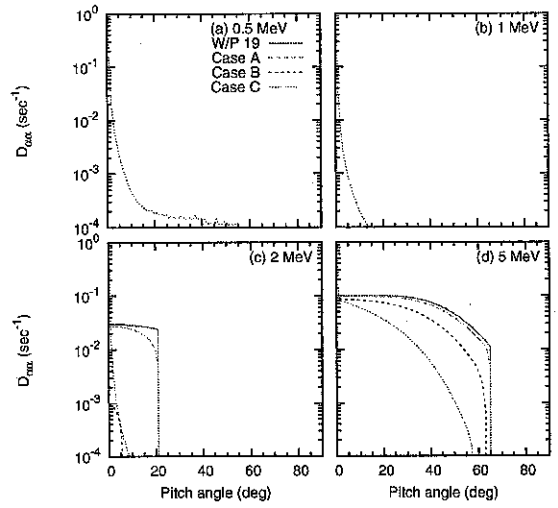
466 **Figure 3.**



467

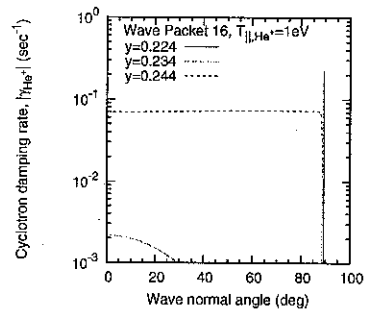
468 **Figure 4.**





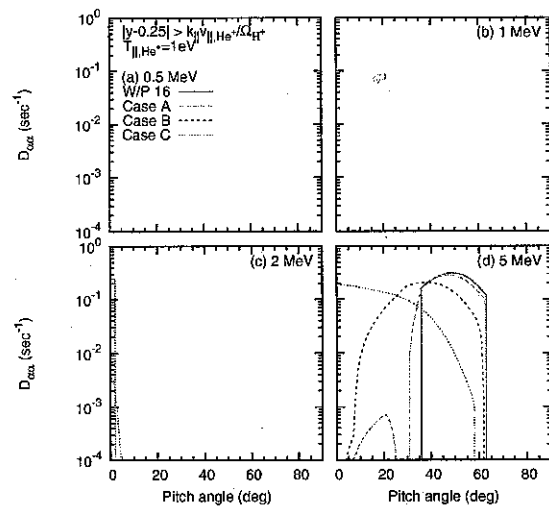
469

470 **Figure 5.**



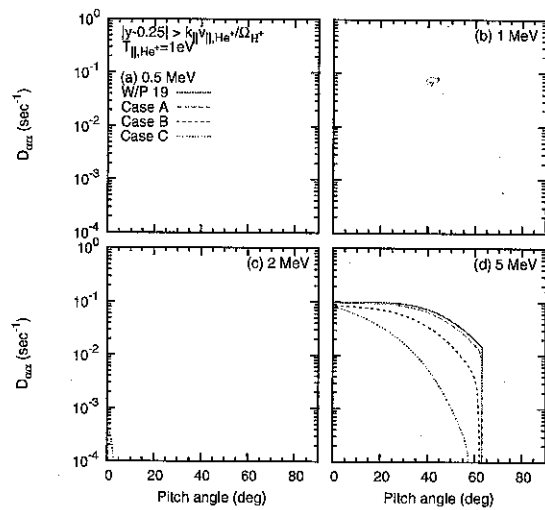
471

472 **Figure 6.**



473

474 Figure 7.



475

476 **Figure 8.**

**Table 1.** Wave Packet and Local Environment Properties Selected From [*Loto'aniu et al.*, 2006]

Wave Packet	$y_m =$ $\omega_m/\Omega_{H^+}$	$\delta y =$ $\delta\omega/\Omega_{H^+}$	$y_{LC} =$ $y_m - \delta y$	$y_{UC} =$ $y_m + \delta y$	$\delta B^2$ nT <sup>2</sup>	$B_0$ nT	$N_e$ cm <sup>-3</sup>
16	0.23	0.01	0.22	0.24	2.21	170.9	17
19	0.22	0.02	0.20	0.24	0.84	160.2	15